Fenofibrate suppresses proliferation and alters cell-cycle progression in SW620 colorectal cancer cells

TATSUYA MORINISHI[1], YASUNORI TOKUHARA[1], FUTOSHI SUIZU[1], AKISHIGE IKEGAME[1], AKIHIRO KONDO[1], SHINICHI TANAKA[2] and EIICHIRO HIRAKAWA[1]

[1]Department of Medical Technology, Kagawa Prefectural University of Health Sciences, Takamatsu, Kagawa 761-0123, Japan; [2]Department of Medical Technology, Kawasaki University of Medical Welfare, Kurashiki, Okayama 701-0193, Japan

Received March 16, 2026; Accepted November 3, 2026

DOI: 10.3892/ol.2026.15959

Abstract. In the present study, the antitumor effects of fenofibrate, a peroxisome proliferator-activated receptor (PPAR)-α agonist, on human colorectal cancer cells were investigated. Treatment of SW620 cells with fenofibrate resulted in a significant, dose-dependent decrease in cell viability. Flow cytometric analysis showed that fenofibrate altered the cell cycle distribution in a concentration-dependent manner: The G0/G1 fraction increased at 12.5 and 25 μM with a concomitant decrease in the S fraction, whereas at 50 μM, the G0/G1 fraction was depleted and both the S and G2/M fractions increased, indicating perturbation of cell cycle progression rather than uniform arrest in a single phase. Annexin V/propidium iodide staining revealed only marginal changes in the apoptotic and necrotic populations, and the combined proportion of early apoptotic, late apoptotic and necrotic cells remained <4% at all tested concentrations, consistent with limited overt cell death. Western blot analysis performed in three independent experiments revealed a concentration-dependent decrease in the expression of the cell cycle regulators Cyclin D1 and Cyclin B1, which was statistically significant at 50 μM. Papanicolaou staining, performed in four independent experiments, revealed a significant, dose-dependent decrease in the mitotic index. These results suggest that fenofibrate suppresses SW620 cell proliferation predominantly through cytostatic effects and concentration-dependent alterations in cell cycle distribution, rather than through marked apoptosis induction. Although this study suggests that fenofibrate could be a potential therapeutic strategy for cancer treatment, further investigation is required to elucidate its underlying molecular mechanisms.

Correspondence to: Dr Tatsuya Morinishi, Department of Medical Technology, Kagawa Prefectural University of Health Sciences, 281-1 Hara, Mure-cho, Takamatsu, Kagawa 761-0123, Japan
E-mail: morinishi@kagawa-puhs.ac.jp

Key words: PPAR-α, colorectal cancer, fenofibrate, apoptosis, cell cycle arrest

Introduction

Colorectal cancer (CRC) is the third most common type of cancer worldwide and the second leading cause of cancer-related mortality, accounting for ~900,000 deaths annually (1). In recent years, it has become clear that metabolic reprogramming plays an important role in the progression of CRC. Increased fatty acid synthesis and lipid metabolism have been observed in advanced CRC, and these metabolic changes have been reported to contribute to the survival and proliferation of tumor cells (2). The standard treatments for CRC include surgery, chemotherapy and radiation therapy. However, these treatments often have significant adverse effects and limitations, particularly in advanced or recurrent cases, highlighting the urgent need for effective therapies. The proliferative capacity of colorectal tumors varies with the degree of differentiation; poorly differentiated tumors generally have a greater metastatic potential and worse prognosis (3). Therefore, there is an urgent need to develop safe and effective drugs that can inhibit colorectal cell proliferation and thereby improve patient outcomes.

Recently, peroxisome proliferator-activated receptors (PPARs) have been implicated in the anticancer response in CRC (4-6). PPARs are nuclear hormone receptors found across multiple species (including humans) that regulate the transcription of genes involved in lipid metabolism, energy homeostasis and storage (7,8). There are three PPAR subtypes-PPAR-α, PPAR-β/δ and PPAR-γ-each with distinct physiological functions (9,10). PPAR-α primarily governs lipid metabolism and energy expenditure (11,12), PPAR-β/δ plays a role in cell proliferation and differentiation (13), and PPAR-γ is involved in adipocyte differentiation and glucose metabolism (14). PPAR-α is a central regulator of lipid metabolism and is involved in metabolic regulation of cancer cells and tumor growth. Notably, these receptors can influence cancer cell proliferation and metastasis; in particular, PPAR-α activation is associated with anticancer effects (7). Fenofibrate, a widely used drug for the treatment of hypercholesterolemia, exerts lipid-lowering effects by activating the PPAR-α receptor (15-17). Fenofibrate is a therapeutic agent for lipid disorders approved by the United States Food and Drug Administration and has a well-established safety profile. In recent years, from a drug-repositioning perspective,

its antitumor effects have attracted attention, and multifaceted anticancer activities, such as cell cycle arrest, induction of apoptosis, and inhibition of invasion and metastasis, have been reported (18,19). Recent studies have shown that fenofibrate inhibits the proliferative capacity of cancer cells in the liver, cervix, breast, stomach and lungs (20-24). However, studies on the effects of fenofibrate on CRC are limited, and the underlying mechanisms remain elusive (6,25).

The aim of this study was to evaluate the antitumor effects of fenofibrate, a PPAR-α agonist, on CRC cells. Specifically, its effects on cell viability, apoptosis, cell cycle distribution and the expression of related proteins were analyzed to elucidate its mechanism of action. The results of this study provide fundamental insights into the potential therapeutic application of fenofibrate for CRC and are expected to contribute to the development of novel treatment strategies.

Materials and methods

Cell culture. SW620 cells (a poorly differentiated human CRC cell line) were purchased from KAC Co., Inc. (cat. no. EC87051203-F0). The cells were cultured in Leibovitz's L-15 medium (Wako Pure Chemical Industries) supplemented with 10% heat-inactivated fetal bovine serum (Biological Industries) and 1% penicillin-streptomycin (Wako Pure Chemical Industries). Cultures were maintained at 37˚C in a humidified atmosphere containing 5% CO_2. The authenticity of the SW620 cells was verified using short tandem repeat profiling. Mycoplasma contamination was routinely tested with a PCR-based detection kit, and all experiments were performed using mycoplasma-free cells. Cells were passaged every 3-4 days at ~80% confluence using 0.25% trypsin-EDTA (Wako Pure Chemical Industries).

Cell proliferation assay. Cell viability was assessed using the MTT Cell Proliferation Assay kit (Cayman Chemical Co.). Cells were seeded in 96-well plates with ~1x10^4 cells/well in 100 μl of medium and incubated for 24 h.

Fenofibrate (TCI Chemicals) was dissolved in dimethyl sulfoxide (DMSO) to prepare a 10-mM stock solution, which was stored at -80˚C until use. Working solutions were freshly prepared by diluting the stock solution to the desired concentrations in culture medium. Equal volumes of the working solutions were added to each well, and the final DMSO concentration was adjusted to 0.1% in all experimental groups, including the vehicle controls.

After treatment with fenofibrate at the indicated concentrations for 48 h, 10 μl of MTT reagent was added to each well and the plates were incubated at 37˚C for 3 h. Subsequently, Crystal Dissolving Solution was added to each well and the plates were incubated for another 6 h at 37˚C to dissolve the formazan crystals. Finally, the optical density was measured at 570 nm using a Model 680 microplate reader (Bio-Rad Laboratories, Inc.). Each condition was assayed in a single well per plate, and the assay was performed in five independent biological experiments on different days (n=5).

Apoptosis analysis. Apoptosis was detected using an Annexin V-FITC Assay Kit (Cayman Chemical Co.) according to the manufacturer's instructions. In brief, the cells were collected and centrifuged at 367 x g for 5 min at room temperature. The pellet was resuspended in 200 μl of 1X Binding Buffer and gently mixed to obtain a single-cell suspension. After additional centrifugation at 367 x g for 5 min at room temperature, the supernatant was removed and the cells were resuspended in 50 μl of Annexin V-FITC/propidium iodide staining solution. The cells were then incubated at room temperature in the dark for 10 min. Subsequently, 150 μl of 1X Binding Buffer was added to each sample and the cells were immediately analyzed by flow cytometry (Cytoflex; Beckman Coulter, Inc.). The analysis was performed in three independent biological experiments (n=3) for each treatment condition.

Cell cycle analysis. The cell cycle distribution was analyzed using a Cell Cycle Phase Determination Kit (Cayman Chemical Co.) according to the manufacturer's instructions. In brief, cells were collected, washed with cold PBS and fixed in 75% ethanol at -20˚C overnight. The fixed cells were washed twice with cold PBS by centrifugation at 500 x g for 5 min at room temperature. Subsequently, 500 μl of DNA staining solution (containing 200 μg/ml RNase A and 20 μg/ml propidium iodide) was added to each sample and cells were incubated at room temperature for 30 min. The stained cells were analyzed by flow cytometry (Cytoflex; Beckman Coulter, Inc.) to determine the cell cycle phase distribution. The analysis was performed in three independent biological experiments (n=3) for each treatment condition.

Western blot analysis. Western blotting was performed as described previously (6). In brief, proteins were separated using 10% SDS-PAGE (Oriental Instruments) and transferred on PVDF membranes (Merck KGaA). Membranes were blocked with 2% skimmed milk (Wako Pure Chemical Industries) at room temperature, then incubated with mouse monoclonal anti-Cyclin D1 (cat. no. SC-8396; 1:200 dilution; Santa Cruz Biotechnology, Inc.), anti-Cyclin B1 (cat. no. SC-166210; 1:200 dilution; Santa Cruz Biotechnology, Inc.) antibodies and rabbit monoclonal anti-β-actin (cat. no. 4970S; 1:5,000 dilution; Cell Signaling Technology, Inc.) antibodies overnight at 4˚C. After washing, the membranes were incubated with horseradish peroxidase-conjugated anti-mouse IgG (cat. no. 7076S; 1:5,000 dilution; Cell Signaling Technology, Inc.) and horseradish peroxidase-conjugated anti-rabbit IgG (cat. no. 7074S; 1:5,000 dilution; Cell Signaling Technology, Inc.) secondary antibodies for 1 h at room temperature. Signals were detected using an enhanced chemiluminescence reagent (Chemi-Lumi One Super; Nacalai Tesque, Inc.). β-actin was used as a loading control. All western blot analyses were performed in three independent biological experiments, each using lysates prepared from separately seeded and treated cultures on different occasions. Band intensities were quantified by densitometry using Fiji/ImageJ software (version 2.18.0; National Institutes of Health), normalized to β-actin and expressed as the target/β-actin ratio.

Immunofluorescence staining. Immunofluorescence staining was performed on the cultured cells. The cells were fixed with 4% paraformaldehyde for 10 min at room temperature, blocked with 2% bovine serum albumin (BSA; Wako Pure Chemical Industries) in PBS and permeabilized with 2% BSA

in PBS containing 0.1% Triton X-100 for 30 min. The cells were incubated for 2 h at room temperature with primary antibodies against cyclin D1 (A-12) (cat. no. SC-8396; 1:200 dilution; Santa Cruz Biotechnology, Inc.), anti-cyclin B (D-1) (cat. no. SC-166210; 1:200 dilution; Santa Cruz Biotechnology, Inc.) and anti-Bcl-2 (C-2) (cat. no. SC-7382; 1:200 dilution; Santa Cruz Biotechnology, Inc.). After three washes with PBS, the cells were incubated for 1 h with an Alexa Fluor 594-conjugated donkey anti-mouse IgG secondary antibody (cat. no. ab150108; Abcam) diluted in 2% BSA in PBS, along with the nuclear counterstain Hoechst 33258 (1 mg/ml; Sigma-Aldrich; Merck KGaA). Finally, the samples were mounted in 80% glycerol in PBS (glycerol; Wako Pure Chemical Industries) and fluorescence signals were observed using a confocal laser scanning microscope (FLUOVIEW FV10i; Olympus Corp.).

Papanicolaou staining. Cell suspensions (2 ml) were centrifuged in a cytospin chamber at 425 x g for 3 min at room temperature to deposit the cells on the slides. All staining steps were performed at room temperature. The cells were then fixed in 95% ethanol for 15 min. The slides were rehydrated with 80 and 50% ethanol and rinsed in water for 30 sec. The cells were stained with Gill's hematoxylin (Muto Pure Chemicals) for 3 min and rinsed with water for 30 sec. The slides were differentiated in 0.5% hydrochloric acid and washed under running water for 5 min. Samples were dehydrated using 50 and 95% ethanol. The cells were subsequently stained with OG-6 (ready-to-use solution; Muto Pure Chemicals) for 2 min, rinsed twice with 95% ethanol and stained with EA-50 (ready-to-use solution; Muto Pure Chemicals) for 3 min, followed by multiple washes in 95 and 100% ethanol. Mitotic cells were morphologically identified by Papanicolaou staining, and at least 1,000 cells were randomly counted for each treatment condition to estimate the mitotic index. This analysis was conducted in four independent biological experiments (n=4) for each treatment condition.

Statistical analysis. Data are expressed as the mean ± standard deviation (SD). One-way analysis of variance was performed to assess differences among the groups. The homogeneity of variance was evaluated using the F-test or Levene and Bartlett tests. Dunnett's multiple-comparisons test was used when variances were equal and the Games-Howell post-hoc multiple comparison test was applied when variances were unequal. Statistical significance was set at P<0.05. All statistical analyses were conducted using JMP Pro (v17; SAS Institute Inc.).

Results

Effects of fenofibrate on SW620 cell viability. Previous studies suggested that fenofibrate reduced the viability and growth of CRC cells (6). However, in preliminary experiments, only a 100 μM concentration was evaluated. In the present study, the effects of a broader concentration range (12.5-100 μM, with DMSO as the vehicle control for all groups) were evaluated. The effect of fenofibrate on SW620 cells was examined using an MTT assay. Relative MTT-based viability, expressed as a percentage of the vehicle control, was 100.0±5.6, 80.5±5.1, 43.6±2.0, 30.5±3.6 and 27.0±3.1% at 0, 12.5, 25, 50 and 100 μM, respectively. Fenofibrate reduced MTT-based viability in a concentration-dependent manner, with significant decreases observed at 12.5 (P<0.001), 25 (P<0.001), 50 (P<0.001) and 100 μM (P<0.001) compared with the vehicle control (Fig. 1; one-way ANOVA followed by Dunnett's multiple-comparisons test).

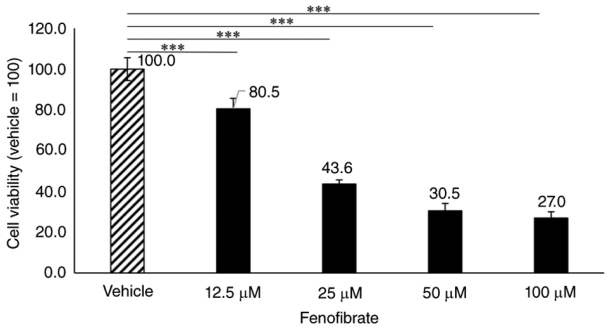


Figure 1. Fenofibrate reduced the MTT-based viability of SW620 cells. SW620 cells were incubated with various fenofibrate concentrations (12.5, 25, 50 and 100 μM) and, DMSO was used as the vehicle control. Cell viability was determined using the MTT assay. Data are presented as the mean ± SD from five independent experiments (n=5). ***P<0.001 vs. vehicle (Dunnett's multiple-comparisons test).

Assessment of apoptosis. SW620 cells were treated with 12.5, 25 and 50 μM fenofibrate (using DMSO as a vehicle control), and the extent of apoptosis was measured using flow cytometry to determine whether the reduction in SW620 cell proliferation caused by fenofibrate was associated with apoptosis. As shown in Fig. 2, fenofibrate treatment produced only small increases in the early apoptotic and necrotic cell populations. The proportion of early apoptotic cells in the vehicle group was 0.77±0.08%, which increased to 1.29±0.29% at 12.5 μM, 2.14±0.12% at 25 μM and 1.67±0.02% at 50 μM fenofibrate (Fig. 2A and B). Similarly, the proportion of necrotic cells in the vehicle group (0.28±0.07%) increased to 0.34±0.06% at 12.5 μM, 0.67±0.06% at 25 μM and 1.30±0.12% at 50 μM fenofibrate (Fig. 2A and C). Immunofluorescence staining of Bcl-2, an anti-apoptotic protein, is shown in Fig. 2D; these images are presented solely to illustrate the subcellular localization of Bcl-2 and were not quantified, and no quantitative inference was drawn from them. The late apoptotic (Annexin V-positive/PI-positive) fraction remained <1% in every group and did not increase in a concentration-dependent manner, accounting for 0.82, 0.91, 0.35 and 0.49% of cells in the vehicle, 12.5, 25 and 50 μM groups, respectively (Fig. 2A). Although some of these increases reached statistical significance (Fig. 2B and C), the combined proportion of early apoptotic, late apoptotic and necrotic cells remained <4% at all tested concentrations, indicating that overt cell death was limited. Together, these results indicate that apoptosis is not the major mechanism of fenofibrate-induced growth suppression in SW620 cells.

Observation of cell cycle changes. Considering that the antiproliferative effect of fenofibrate may involve mechanisms beyond apoptosis, its impact on the cell cycle was examined. SW620 cells were treated with 12.5, 25 and 50 μM fenofibrate (with DMSO as the vehicle control) and analyzed using

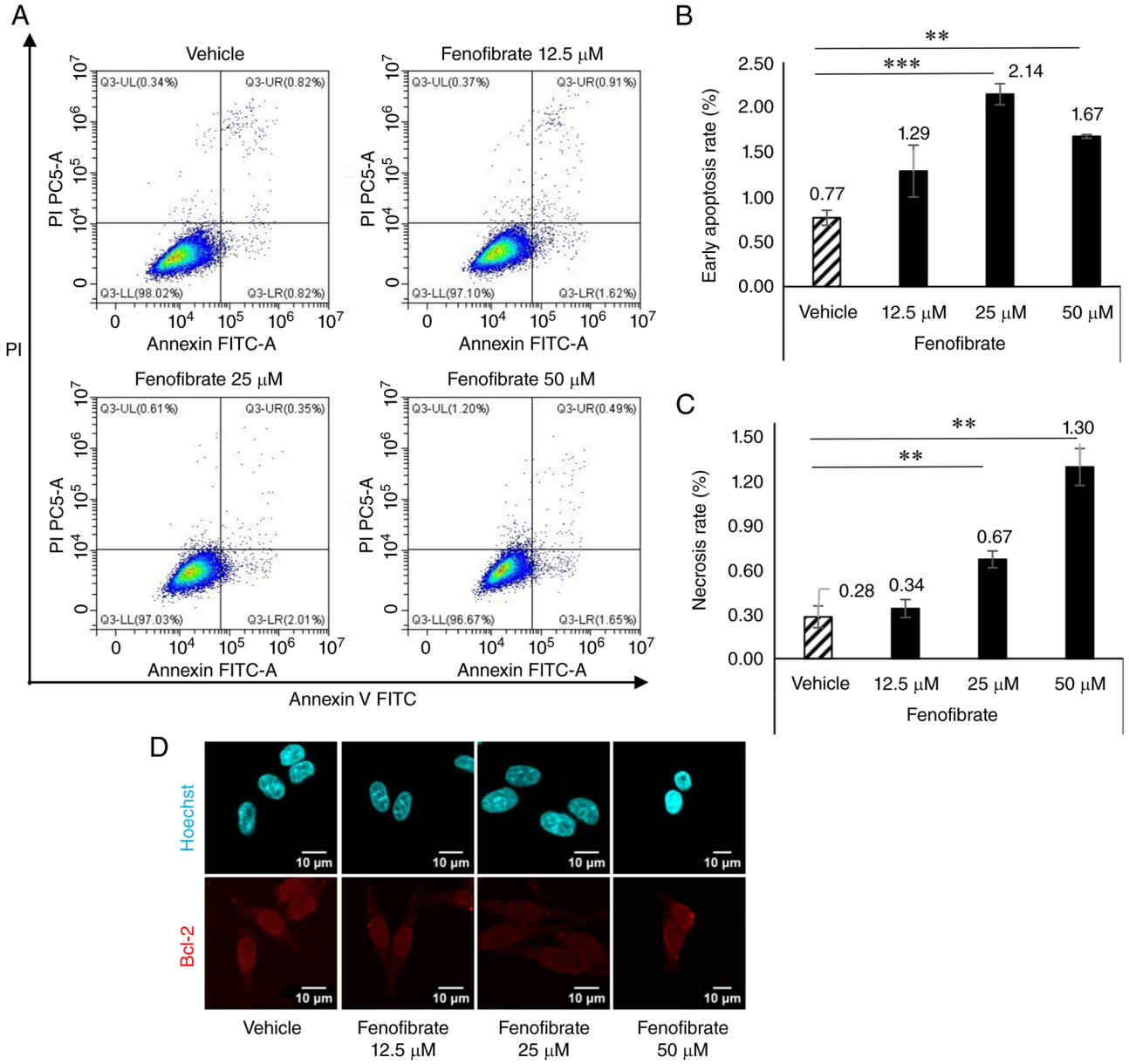


Figure 2. Assessment of apoptosis in SW620 cells treated with fenofibrate. (A) SW620 cells were treated with fenofibrate at concentrations of 12.5, 25 and 50 μM, using DMSO as the vehicle control. The cells were then subjected to Annexin V-FITC and PI staining. Representative flow cytometry dot plots are shown, with the percentage of cells in each quadrant indicated; the late apoptotic (Annexin V-positive/PI-positive) population corresponds to the upper right quadrant. Percentages of (B) early apoptotic and (C) necrotic cells were quantified. Data in panels B and C are presented as the mean ± SD from three independent experiments (n=3). **P<0.01 and ***P<0.001 vs. vehicle (Dunnett's multiple-comparisons test and Games-Howell post-hoc multiple-comparisons test). (D) Representative confocal immunofluorescence images showing the subcellular localization of Bcl-2 (red), with nuclei counterstained with Hoechst 33258 (cyan). Quantitative fluorescence analysis was not performed because of the limited number of available images and partial fluorescence fading in the archived samples (scale bars, 10 μm). PI, propidium iodide.

flow cytometry. Flow cytometry revealed a dose-dependent shift in the cell cycle distribution. Compared to the vehicle (G0/G1 44.1±0.4%, S 31.0±0.9%, G2/M 24.7±1.2%), treatment with 12.5 μM fenofibrate increased the G0/G1 fraction to 65.9±0.4% and reduced the S and G2/M fractions to 14.4±0.1 and 19.5±0.5%, respectively. At 25 μM, the G0/G1 fraction remained elevated (53.3±0.5%), while the S fraction decreased further (6.8±0.5%), and the G2/M fraction increased (39.9±0.3%). At 50 μM, the G0/G1 fraction decreased to 9.0±0.6%, and both S and G2/M fractions increased (41.4±1.2 and 49.6±1.3%, respectively). These data indicate a concentration-dependent perturbation of the cell cycle distribution, rather than a uniform checkpoint arrest (Fig. 3A and B). The expression levels of key cell cycle regulators was assessed by western blotting in three independent biological experiments, with β-actin used as a loading control (Fig. 4B and C). Fenofibrate decreased the expression of both cyclins in a concentration-dependent manner. The Cyclin D1/β-actin ratio was 0.092±0.036 in vehicle-treated cells and 0.074±0.024, 0.067±0.035 and 0.017±0.008 at 12.5, 25 and 50 μM, respectively, and the Cyclin B1/β-actin ratio was 0.128±0.053 in vehicle-treated cells and 0.094±0.056, 0.045±0.037 and 0.005±0.006 at the same concentrations (mean ± SD, n=3). Compared with the

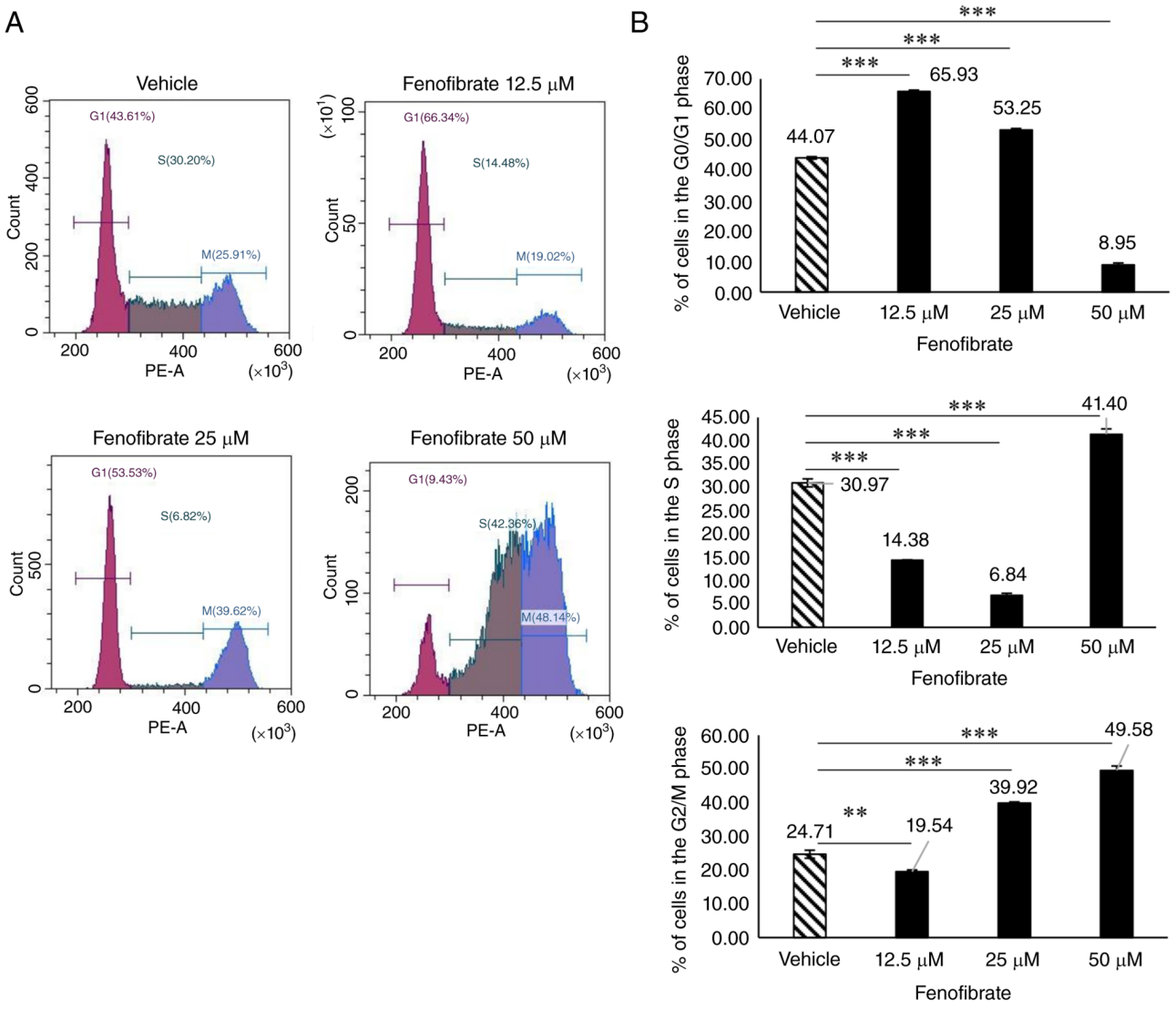


Figure 3. Fenofibrate alters the cell cycle distribution in SW620 cells. (A) SW620 cells were treated with fenofibrate at concentrations of 12.5, 25 and 50 μM, using DMSO as the vehicle control. Flow cytometry was performed to assess the cell cycle distribution, which was visually represented as the proportions of cells in the G0/G1, S and G2/M phases. (B) The proportions of cells in the different phases were quantified. Data are presented as the mean ± SD from three independent experiments (n=3). **P<0.01 and ***P<0.001 vs. vehicle (Dunnett's multiple-comparisons test and Games-Howell post-hoc multiple-comparisons test).

vehicle control, 50 μM fenofibrate significantly reduced both Cyclin D1 (P=0.027) and Cyclin B1 (P=0.020), whereas the reductions at 12.5 and 25 μM did not reach statistical significance (one-way ANOVA followed by Dunnett's multiple-comparisons test). Immunofluorescence staining was performed to examine the subcellular localization of these proteins, showing that Cyclin D1 was predominantly localized in the nucleus (Fig. 4A).

Morphological observation of cells. Papanicolaou staining revealed a concentration-dependent decrease in the proportion of mitotic SW620 cells. Based on random counts of at least 1,000 cells per treatment condition in each of the four independent experiments (n=4), the mitotic index decreased from 3.17±0.44% in vehicle-treated cells to 2.42±0.75, 0.31±0.12 and 0.47±0.42% following treatment with 12.5, 25 and 50 μM fenofibrate, respectively. The reduction was statistically significant at 25 and 50 μM, whereas the change at 12.5 μM did not reach significance (mean ± SD, n=4; significance and statistical test are indicated in the figure legend) (Fig. 5).

Discussion

This study demonstrated that fenofibrate, a PPARα agonist, suppresses the proliferation of SW620 CRC cells predominantly through cytostatic mechanisms accompanied by concentration-dependent alterations in cell cycle distribution, with minimal apoptosis induction. The results showed that fenofibrate reduced MTT-based viability of SW620 cells in a concentration-dependent manner. Previous studies have reported that fenofibrate exerts antitumor effects in colon cancer by inducing apoptosis and altering the cell cycle distribution (25). For example, fenofibrate treatment suppresses prostate tumor growth (26); promotes apoptosis in lung cancer cells (27); inhibits oral tumorigenesis (17); and induces cell cycle arrest or apoptosis in cervical (24), liver (28), gastric (20)

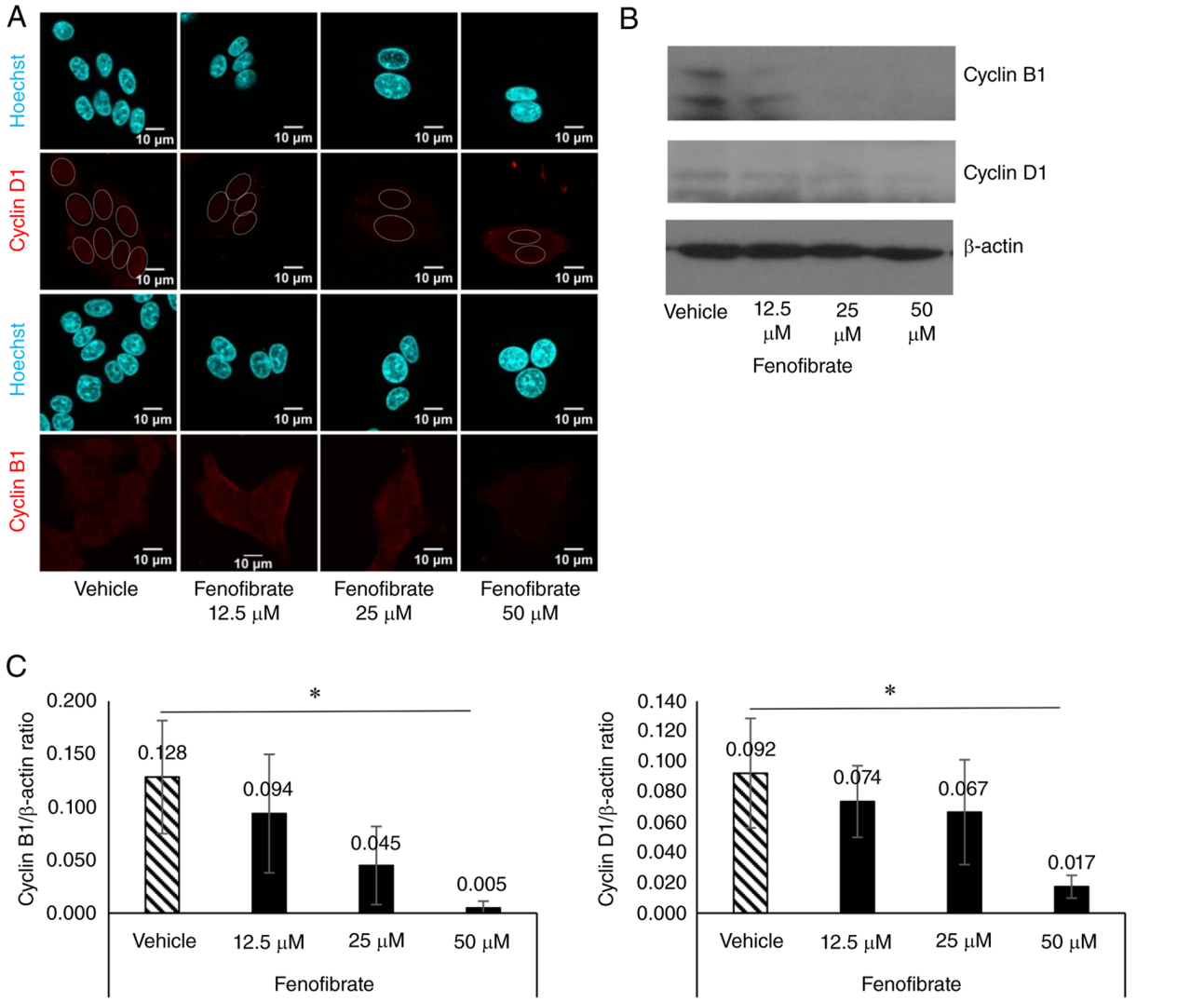


Figure 4. Fenofibrate decreases Cyclin B1 and Cyclin D1 expression in SW620 cells. SW620 cells were treated with fenofibrate at concentrations of 12.5, 25, and 50 μM, using DMSO as the vehicle control. (A) The subcellular localization of Cyclin D1 and Cyclin B1 was examined using confocal fluorescence microscopy with Hoechst counterstaining, and all treatment groups were imaged under identical settings. Cyclin D1 is localized predominantly in the nucleus, as highlighted by the white dashed outline. Cyclin B1 expression was also detected within the cells. Representative immunofluorescence images are presented. Quantitative fluorescence analysis was not performed because of the limited number of available images and partial fluorescence fading in archived samples (scale bars, 10 μm). (B) Representative western blots of Cyclin B1 and Cyclin D1 from three independent biological experiments, with β-actin used as a loading control. (C) Densitometric quantification of the blots, expressed as the target/β-actin ratio (mean ± SD of three independent biological experiments, n=3). *P<0.05 vs. vehicle, determined by one-way analysis of variance followed by Dunnett's multiple-comparisons test.

and endometrial (29) cancer cells. However, CRC has distinct metabolic characteristics compared with other tumor types. Previous studies have demonstrated that CRC undergoes metabolic reprogramming during tumor progression, with early-stage tumors exhibiting enhanced glycolytic activity. By contrast, advanced CRCs exhibit increased lipid synthesis and fatty acid metabolism, including the upregulation of fatty acid synthase (2). In addition, PPARα signaling has been implicated in the regulation of lipid metabolism and tumor progression in CRC (30).

SW620 cells are derived from metastatic CRC and may exhibit metabolic features associated with advanced-stage disease (31). In this context, the present findings show that fenofibrate influences CRC cell viability and cell cycle distribution; whether CRC-associated metabolic pathways contribute to these effects was not addressed experimentally in the present study and remains to be determined. Compared with reports on other malignancies, this study highlights the potential relevance of lipid metabolism-related mechanisms in CRC. However, additional mechanistic studies are necessary to clarify the precise role of PPARα-dependent signaling.

In the present study, the effects of fenofibrate on apoptosis and cell cycle progression were examined using flow cytometry and the mitotic phases were assessed using Papanicolaou staining.

The early apoptotic and necrotic fractions increased only modestly following fenofibrate treatment; the late apoptotic fraction remained <1% and showed no concentration-dependent increase, and the combined proportion of early apoptotic, late apoptotic and necrotic cells remained <4% at all concentrations tested. Notably, in other cancer models, fenofibrate induces apoptosis by upregulating pro-apoptotic Bad and downregulating anti-apoptotic Bcl-xL and Survivin, thereby activating caspase-3 (18). In SW620 cells, by contrast, the

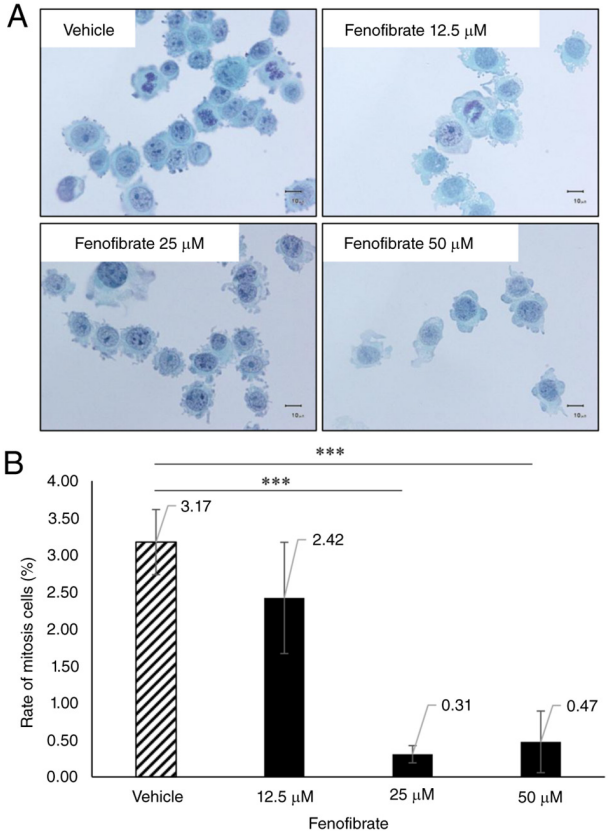


Figure 5. Fenofibrate induced morphological changes and reduced the mitotic index in SW620 cells. SW620 cells were treated with fenofibrate at concentrations of 12.5, 25 and 50 μM, using DMSO as the vehicle control. (A) Representative Papanicolaou-stained images of SW620 cells for each treatment condition (scale bars, 10 μm). (B) At least 1,000 cells were randomly counted for each treatment condition in each of four independent biological experiments to estimate the mitotic index. The graph compares the percentage of mitotic cells between the vehicle control and fenofibrate-treated groups. Data are presented as the mean ± SD (n=4). ***P<0.001 vs. vehicle (Dunnett's multiple-comparisons test); the mitotic index at 12.5 μM did not differ significantly from the vehicle control.

combined proportion of early apoptotic, late apoptotic and necrotic cells remained <4% at all concentrations tested, consistent with a predominantly cytostatic rather than a pro-apoptotic response. However, the present study had several limitations. First, apoptosis was evaluated solely by Annexin V/propidium iodide flow cytometry. Antibodies against total caspase-3/7, poly(ADP ribose) polymerase (PARP) and cleaved PARP were not available during the study period, and an external positive control for apoptosis induction was not included. The conclusion that fenofibrate does not induce substantial apoptosis in SW620 cells under the present conditions therefore rests on the flow cytometric data alone, and a residual apoptotic component cannot be formally excluded. Second, although fenofibrate is a known PPAR-α agonist, the dependence of the observed effects on PPAR-α was not directly tested using a PPAR-α antagonist or gene silencing, and a PPAR-α-independent contribution cannot be excluded. Therefore, the precise molecular basis for the predominantly cytostatic effect of fenofibrate in SW620 cells remains elusive. Third, only a single CRC cell line (SW620) was used, limiting the generalizability of the present results. Therefore, additional investigations using multiple CRC cell lines and *in vivo* models are required to confirm the antitumor effects of fenofibrate in CRC.

Additionally, cell cycle alterations were explored. Flow cytometry revealed marked concentration-dependent shifts in cell cycle phase distribution following fenofibrate treatment. Consistent with the flow cytometric analysis, fenofibrate treatment altered the distribution of SW620 cells across different cell cycle phases in a concentration-dependent manner. At 12.5 μM, the G0/G1 fraction increased, whereas the S and G2/M fractions decreased, suggesting enrichment of cells in the G0/G1 phase. By contrast, higher concentrations produced distinct alterations in cell cycle distribution, including a marked reduction in the S fraction at 25 μM and increases in both S and G2/M fractions at 50 μM. These findings indicate that fenofibrate disrupts cell cycle progression in SW620 cells rather than inducing uniform arrest in a single phase. The increased G0/G1 fraction observed at lower concentrations was associated with reduced Cyclin D1 expression, suggesting the possible involvement of G1-phase regulatory mechanisms.

Consistent with these cell-cycle changes, fenofibrate has also been reported to cause arrest in the S and G2/M phases in Hep3B hepatocellular carcinoma cells, with decreased Cyclin D1 and E levels and an increase in Cyclin A (21) rather than Cyclin B. Previous mechanistic studies have shown that fenofibrate can induce G1 arrest by suppressing cyclin-cyclin-dependent kinase (CDK) activity. For instance, Kong *et al* (25) demonstrated that fenofibrate-induced PPARα activation leads to downregulation of Cyclin-CDK complexes, upregulation of CDK inhibitor 2A and G1/S arrest through the retinoblastoma protein/E2F transcription factor pathway. Consistent with this, the present study found that Cyclin D1, which drives the G1/S transition and was predominantly nuclear, decreased dose-dependently, and Cyclin B1 (which controls the G2/M checkpoint) showed a marked concentration-dependent reduction that reached statistical significance at 50 μM. Therefore, the downregulation of Cyclin D1 at lower fenofibrate concentrations may have contributed to the accumulation of cells in the G0/G1 phase. By contrast, the pronounced reduction in Cyclin B1 is consistent with impaired progression through G2/M at higher concentrations. These findings suggest that fenofibrate exerts concentration-dependent effects on distinct cell cycle phases, providing a mechanistic explanation for the flow cytometry results. A further limitation is that quantitative analysis of immunofluorescence staining could not be reliably performed because of the limited number of available images and partial fluorescence fading of the archived samples. Therefore, the immunofluorescence findings should be interpreted as representative qualitative observations.

Additionally, cellular morphology was examined using Papanicolaou staining, which revealed that higher fenofibrate concentrations led to a decreased percentage of mitotic cells in SW620 cultures, as quantified by random field counts. These observations align with the flow cytometry data of the present study; at 12.5 μM, cells accumulated predominantly in the G0/G1 phase, whereas at 25 μM, many cells accumulated in the G2/M phase with a concomitant reduction in the S phase. The increase in the G2/M population at 25 μM, together with the marked decrease in mitotic figures, is consistent with impaired progression through mitosis. At 50 μM, both the S

and G2/M fractions were elevated, and the G0/G1 fraction was depleted, accompanied by a low mitotic index, indicating that few cells completed division. These results indicate that fenofibrate markedly reduced the number of cells completing mitosis. Similarly, fenofibrate treatment reduced the number of mitotic HeLa cervical cancer and MDA-MB-231 breast cancer cells, consistent with induction of cell cycle arrest and apoptosis (32).

In conclusion, the present study demonstrated that fenofibrate suppresses the proliferation of SW620 CRC cells, predominantly through cytostatic effects and disruption of cell cycle progression. These antiproliferative effects were concentration-dependent and accompanied by altered cell cycle distribution, reduced expression of Cyclin D1 and Cyclin B1, and a decreased number of mitotic cells, whereas apoptosis induction was minimal. Collectively, these findings indicate that fenofibrate predominantly exerts cytostatic antiproliferative effects in CRC cells by modulating pathways involved in cell survival and cell cycle regulation. Although further studies are required to clarify the underlying molecular mechanisms and role of PPARα signaling, the present results support the potential repositioning of fenofibrate as a therapeutic candidate for CRC.

Acknowledgements

Not applicable.

Funding

This research was supported by the Japan Society for the Promotion of Science KAKENHI Grant-in-Aid for Early-Career Scientists (grant no. JP24K18984), which supported the investigation of the antitumor effects and signaling mechanisms of fenofibrate in CRC cells. This study was also supported in part by a grant from the Charitable Trust MIU Foundation Memorial Fund, which contributed to the experimental analyses, including flow cytometry and immunofluorescence experiments, data analysis and manuscript preparation.

Availability of data and materials

The data generated in the present study may be requested from the corresponding author.

Authors' contributions

TM and EH conceived and designed the study. TM performed the experiments, data analysis and literature search, and drafted the manuscript. YT and FS contributed to the experimental design and data interpretation, and reviewed and edited the manuscript. ST and EH provided critical advice on the experimental procedures and interpretation of the results, and critically revised the manuscript. AI and AK supervised and contributed to all aspects of flow cytometry experiments, including data collection, analysis and interpretation. TM and FS confirm the authenticity of all the raw data. All authors have read and approved the final version of the manuscript.

Ethics approval and consent to participate

Not applicable.

Patient consent for publication

Not applicable.

Competing interests

The authors declare that they have no competing interests.

References

1. Sung H, Ferlay J, Siegel RL, Laversanne M, Soerjomataram I, Jemal A and Bray F: Global cancer statistics 2020: GLOBOCAN estimates of incidence and mortality worldwide for 36 cancers in 185 countries. CA Cancer J Clin 71: 209-249, 2021.
2. Zhang J, Zou S and Fang L: Metabolic reprogramming in colorectal cancer: Regulatory networks and therapy. Cell Biosci 13: 25, 2023.
3. Compton CC: Colorectal carcinoma: Diagnostic, prognostic, and molecular features. Mod Pathol 16: 376-388, 2003.
4. Theocharis S, Giaginis C, Parasi A, Margeli A, Kakisis J, Agapitos E and Kouraklis G: Expression of peroxisome proliferator-activated receptor-gamma in colon cancer: Correlation with histopathological parameters, cell cycle-related molecules, and patients' survival. Dig Dis Sci 52: 2305-2311, 2007.
5. Tsukahara T, Haniu H and Matsuda Y: PTB-associated splicing factor (PSF) is a PPARgamma-binding protein and growth regulator of colon cancer cells. PLoS One 8: e58749, 2013.
6. Morinishi T, Tokuhara Y, Ohsaki H, Ibuki E, Kadota K and Hirakawa E: Activation and expression of peroxisome Proliferator-Activated receptor alpha are associated with tumorigenesis in colorectal carcinoma. PPAR Res 2019: 7486727, 2019.
7. Pozzi A, Ibanez MR, Gatica AE, Yang S, Wei S, Mei S, Falck JR and Capdevila JH: Peroxisomal proliferator-activated receptor-alpha-dependent inhibition of endothelial cell proliferation and tumorigenesis. J Biol Chem 282: 17685-17695, 2007.
8. Issemann I and Green S: Activation of a member of the steroid hormone receptor superfamily by peroxisome proliferators. Nature 347: 645-650, 1990.
9. Yokoyama Y, Xin B, Shigeto T, Umemoto M, Kasai-Sakamoto A, Futagami M, Tsuchida S, Al-Mulla F and Mizunuma H: Clofibric acid, a peroxisome proliferator-activated receptor alpha ligand, inhibits growth of human ovarian cancer. Mol Cancer Ther 6: 1379-1386, 2007.
10. Ramanan S, Kooshki M, Zhao W, Hsu FC and Robbins ME: PPARalpha ligands inhibit radiation-induced microglial inflammatory responses by negatively regulating NF-kappaB and AP-1 pathways. Free Radic Biol Med 45: 1695-1704, 2008.
11. Bougarne N, Weyers B, Desmet SJ, Deckers J, Ray DW, Staels B and De Bosscher K: Molecular actions of PPARα in lipid metabolism and inflammation. Endocr Rev 39: 760-802, 2018.
12. Lee SY, Shin MJ, Choi SM, Kim DK, Choi MG, Kim JS, Suh DS, Kim JH and Kim SJ: Role of peroxisome Proliferator-activated receptor α-dependent mitochondrial metabolism in ovarian cancer stem cells. Int J Mol Sci 25: 11760, 2024.
13. Müller R, Rieck M and Müller-Brüsselbach S: Regulation of cell proliferation and differentiation by PPARbeta/delta. PPAR Res 2008: 614852, 2008.
14. Choi SS, Cha BY, Iida K, Lee YS, Yonezawa T, Teruya T, Nagai K and Woo JT: Artepillin C, as a PPARγ ligand, enhances adipocyte differentiation and glucose uptake in 3T3-L1 cells. Biochem Pharmacol 81: 925-933, 2011.
15. Staels B, Dallongeville J, Auwerx J, Schoonjans K, Leitersdorf E and Fruchart JC: Mechanism of action of fibrates on lipid and lipoprotein metabolism. Circulation 98: 2088-2093, 1998.
16. Soska V: Present status of fibrates in the treatment of hyperlipoproteinemias. Vnitr Lek 45: 438-440, 1999 (In Czech).
17. Su TR, Yu CC, Chao SC, Huang CC, Liao YW, Hsieh PL, Yu CH and Lin SS: Fenofibrate diminishes the self-renewal and metastasis potentials of oral carcinoma stem cells through NF-κB signaling. J Formos Med Assoc 121: 1900-1907, 2022.

18. Lian X, Wang G, Zhou H, Zheng Z, Fu Y and Cai L: Anticancer properties of fenofibrate: A repurposing use. J Cancer 9: 1527-1537, 2018.
19. Ling H, Luoma JT and Hilleman D: A review of currently available fenofibrate and fenofibric acid formulations. Cardiol Res 4: 47-55, 2013.
20. Chen L, Peng J, Wang Y, Jiang H, Wang W, Dai J, Tang M, Wei Y, Kuang H, Xu G and Zhou F: Fenofibrate-induced mitochondrial dysfunction and metabolic reprogramming reversal: The anti-tumor effects in gastric carcinoma cells mediated by the PPAR pathway. Am J Transl Res 12: 428-446, 2020.
21. You BJ, Hour MJ, Chen LY, Luo SC, Hsu PH and Lee HZ: Fenofibrate induces human hepatoma Hep3B cells apoptosis and necroptosis through inhibition of thioesterase domain of fatty acid synthase. Sci Rep 9: 3306, 2019.
22. Sun J, Zheng Z, Chen Q, Pan Y, Quan M and Dai Y: Fenofibrate potentiates chemosensitivity to human breast cancer cells by modulating apoptosis via AKT/NF-κB pathway. Onco Targets Ther 12: 773-783, 2019.
23. Piwowarczyk K, Kwiecień E, Sośniak J, Zimoląg E, Guzik E, Sroka J, Madeja Z and Czyż J: Fenofibrate interferes with the diapedesis of lung adenocarcinoma cells through the interference with Cx43/EGF-dependent intercellular signaling. Cancers 10: 363, 2018.
24. Song SY, Lee SY, Ko YB, Kim J, Choi TY, Lee KH, Yoo HJ and Yuk JM: Fenofibrate exerts anticancer effects on human cervical cancer HeLa cells via caspase-dependent apoptosis and cell cycle arrest. Gynecol Obstet Invest 87: 79-88, 2022.
25. Kong R, Wang N, Han W, Bao W and Lu J: Fenofibrate exerts antitumor effects in colon cancer via regulation of DNMT1 and CDKN2A. PPAR Res 2021: 6663782, 2021.
26. Tao T, Zhao F, Xuan Q, Shen Z, Xiao J and Shen Q: Fenofibrate inhibits the growth of prostate cancer through regulating autophagy and endoplasmic reticulum stress. Biochem Biophys Res Commun 503: 2685-2689, 2018.
27. Wang MS, Han QS, Jia ZR, Chen CS, Qiao C, Liu QQ, Zhang YM, Wang KW, Wang J, Xiao K, *et al*: PPARα agonist fenofibrate relieves acquired resistance to gefitinib in non-small cell lung cancer by promoting apoptosis via PPARα/AMPK/AKT/FoxO1 pathway. Acta Pharmacol Sin 43: 167-176, 2022.
28. Li B, Jiang HY, Wang ZH, Ma YC, Bao YN and Jin Y: Effect of fenofibrate on proliferation of SMMC-7721 cells via regulating cell cycle. Hum Exp Toxicol 40: 1208-1221, 2021.
29. Saidi SA, Holland CM, Charnock-Jones DS and Smith SK: In vitro and in vivo effects of the PPAR-alpha agonists fenofibrate and retinoic acid in endometrial cancer. Mol Cancer 5: 13, 2006.
30. Wang C, Lv T, Jin B, Li Y and Fan Z: Regulatory role of PPAR in colorectal cancer. Cell Death Discov 11: 28, 2025.
31. Leibovitz A, Stinson JC, McCombs WB III, McCoy CE, Mazur KC and Mabry ND: Classification of human colorectal adenocarcinoma cell lines. Cancer Res 36: 4562-4569, 1976.
32. Li T, Zhang Q, Zhang J, Yang G, Shao Z, Luo J, Fan M, Ni C, Wu Z and Hu X: Fenofibrate induces apoptosis of triple-negative breast cancer cells via activation of NF-κB pathway. BMC Cancer 14: 96, 2014.

Copyright © 2026 Morinishi et al. This work is licensed under a Creative Commons Attribution-NonCommercial-NoDerivatives 4.0 International (CC BY-NC-ND 4.0) License.